Research in Pharmaceutical Sciences, February 2021; 16(1): 79-93
Received: 26-12-2019
Peer Reviewed: 13-05-2020
Revised: 16-06-2020
Accepted: 30-11-2020
Published: 30-12-2020

School of Pharmacy & Pharmaceutical Sciences
Isfahan University of Medical Sciences

Original Article

Chitosan/tripolyphosphate nanoparticles in active and passive microchannels

Mona Akbari[1,2], Zohreh Rahimi[2,3,*], and Masoud Rahimi[4]

[1]Department of Chemical Engineering, University of Hormozgan, Bandar Abbas, I.R. Iran.
[2]Medical Biology Research Center, Kermanshah University of Medical Sciences, Kermanshah, I.R. Iran.
[3]Department of Clinical Biochemistry, Medical School, Kermanshah University of Medical Sciences, Kermanshah, I.R. Iran.
[4]CFD Research Center, Chemical Engineering Department, Razi University, Kermanshah, I.R. Iran.

Abstract

Background and purpose: In recent years, the interest in chitosan nanoparticles has increased due to their application, especially in drug delivery. The main aim of this work was to find a suitable method for simulating pharmaceutical nanoparticles with computational fluid dynamics (CFD) modeling and use it for understanding the process of nanoparticle formation in different types of microchannels.
Experimental approach: Active and passive microchannels were compared to find the advantages and disadvantages of each system. Twenty-eight experiments were done on microchannels to quantify the effect of 4 parameters and their interactions on the size and polydispersity index (PDI) of nanoparticles. CFD was implemented by coupling reactive kinetics and the population balance method to simulate the synthesis of chitosan/tripolyphosphate nanoparticles in the microchannel.
Findings/Results: The passive microchannel had the best performance for nanoparticle production. The most uniform microspheres and the narrowest standard deviation (124.3 nm, PDI = 0.112) were achieved using passive microchannel. Compared to the active microchannel, the size and PDI of the nanoparticles were 28.7% and 70.5% higher for active microchannels, and 55.43% and 105.3% higher for simple microchannels, respectively. Experimental results confirmed the validity of CFD modeling. The growth and nucleation rates were determined using the reaction equation of chitosan and tripolyphosphate.
Conclusion and implications: CFD modeling by the proposed method can play an important role in the prediction of the size and PDI of chitosan/tripolyphosphate nanoparticles in the same condition and provide a new perspective for studying the production of nanoparticles by numerical methods.

Keywords: CFD modeling; Chitosan; Microchannel; Nanoparticles; Population balance method.

INTRODUCTION

In recent years, nanotechnology has been grown increasingly in many different fields, especially drug delivery (1,2). Because of the high surface to volume ratio, this technology can modify many important properties in drug delivery such as solubility, drug side effects, drug release, cellular uptake, immunogenicity, and blood circulation half-life. Numerous materials have been investigated to produce nanoparticle-based therapeutics, such as proteins, polymers, lipids, and, so on. Among many types of nanoparticles used for drug delivery, polymers are one of the most popular nanocarriers that have high potential in a variety of biomedical applications comprising treatment of cancer, diabetes, pain, asthma, allergy, infections, etc.

Chitosan (CS) is a natural polymer that is derived from the partial deacetylation of the acetyl group in chitin (3). This polysaccharide has been widely applied for gene and drug delivery (4,5), cell culture, tissue engineering, and wound healing (6).

* Corresponding author: Z. Rahimi
Tel: +98-8334274882, Fax: +98-8334276471
Email: zrahimi@kums.ac.ir

Access this article online

Website: http://rps.mui.ac.ir

DOI: 10.4103/1735-5362.305191

It is non-toxic, biocompatible, biodegradable, bacteriostatic, and non-immunogenic. In addition, because of its high mechanical strength, CS is used for producing gels, membranes, scaffolds, fibers, and micro- and nanoparticles. Besides, the possibility of chemical modification in chitosan molecules provides a suitable carrier for specific desired applications. There are several techniques to formulate CS nanoparticles, comprising co-precipitation, solvent evaporation, coacervation, microemulsion, and ionotropic gelation (7). Ionotropic gelation is based on ionic crosslinking between amine groups of CS and negatively charged small molecules like phosphates and nitrates (8). This method is gaining a great deal of attention because of fabrication in aqueous solution, mild condition, low costs, and avoiding the use of dangerous organic solvents.

For biomedical applications, the main challenge is how to synthesis nanoparticles by controlling their physicochemical properties like size, charge, and polydispersity (9,10). Thus, the nanoparticle fabrication method should be reproducible and reliable. Unfortunately, the simple bulk method is not reproducible and produces polydisperse nanoparticles.

In order to solve the above problem, microfluidic devices have been proposed. Microfluidic systems, miniaturized devices with small volume, have attracted growing attention because of their properties including high surface-to-volume ratio, easy-to-use platforms, continuous flow, low cost, improved analysis times, and accuracy (11-14). These features contribute to the microfluidic devices to have more control over the production of nanoparticles. Microchannels provide high mass transfer compared to batch mixing and produce nanoparticles with controlled size and a narrow polydispersity index (PDI) (15). Unlike macro-scale fluidic devices, in microfluidic systems, diffusion is the dominant method for achieving a homogeneous solution. In order to obtain a more surface-to-volume ratio and to enhance mass transfer efficiency, microfluidic devices can use external turbulence (active microchannel) or microstructures (passive microchannel) on the way of passing flow (12-14,16-18).

Despite extensive attention to the synthesis of pharmaceutical nanoparticles by various processes, the simulation of nanoparticle synthesis with numerical methods is rarely reported. One of the best methods for understanding the process and behavior of fluid is using simulation methods such as computational chemistry approaches (19-22) and computational fluid dynamics (CFD) approach. CFD, an effective tool to display complex fluid behaviors, has also been applied in recent years to explain particle phenomena (23). With an overview of previous works, it can be seen that CFD modeling was used for the investigation of nanoparticles produced using crystallization (24). The method of producing chitosan/tripolyphosphate (CS/TPP) nanoparticles is based on ionic reactions. So, simulation of polymeric nanoparticles in a continuous process like microchannel is a new method due to the lack of appropriate reaction kinetics data. Also, exploring the mechanism of synthesis CS/TPP nanoparticles is necessary to reach a valid model. de Carvalho *et al.* presented a stoichiometric ratio for CS/TPP ionic reaction that provides important information to understand the mechanism of the reaction (25). But the kinetics of nanoparticle formation is not yet well known.

By reviewing the scientific literature, it can be seen that few studies have been carried out on the production of CS nanoparticles in the microchannel (26-29). These works showed the advantages of producing nanoparticles in the microchannels compared to the conventional methods. The objective of the present study is to compare different types of microchannels and demonstrate the advantages and disadvantages of each type. In addition, simulation of CS-nanoparticle formation is a new field due to a lack of experimental information about reaction kinetics. This work aimed to provide a successful simulation method for the microfluidic-assisted formation of CS nanoparticles through ionic reaction with TPP. Simple, active, and passive microchannels were used to compare nanoparticle formation. The CFD modeling was established based on assuming the classic reactions for polymeric interaction. The kinetic constants were calculated by experimental works for

nucleation and growth rates and then were compiled by user-defined functions to model as the terms of the population balance method. First, the optimum condition was obtained by experimental results of microchannels and then, CFD modeling was performed to predict nanoparticle size and PDI.

MATERIALS AND METHODS

Materials

Low molecular weight chitosan hydrochloride was purchased from Sigma-Aldrich Chemical Co. USA (75% to 85% degree of deacetylation, the viscosity of 20 to 300 cP, average molecular weight ~ 50 kDa, Cat. No.: 448869). The degree of deacetylation for chitosan was 86.6%. Sodium tripolyphosphate and sodium hydroxide were obtained from Merck Inc (Germany).

Synthesis of CS/TPP nanoparticles

CS/TPP nanoparticles were synthesized by the ionotropic gelation method that was first presented by Calvo *et al.* (30). The CS was dissolved in 1% w/v acetic acid solution at different concentrations and kept overnight under magnetic stirring at room temperature. The pH of CS solution was increased to 4.7 by 1 N NaOH solution. TPP was dissolved in deionized water and its pH was adjusted to 4.7. Both solutions were filtered through a 0.45 µm Biofil syringe filter. In order to remove the effect of pH on the synthesis of nanoparticles, pH values were set at 4.7 in all experiments. In this way, pH did not make confusion in results.

A schematic diagram of the experimental setup is depicted in Fig. 1. The microchannels were built of two spinal needles with dimensions of 22 and 26 G. As illustrated in Fig. 1, needles were placed inside together to create a two-inlet microchannel. The CS and TPP solutions were injected into A and B inlets using two syringe pumps (SP1000, FNM Co., Iran). Solutions joined together, mixing occurred in the larger channel, and nanoparticles were fabricated. Finally, nanoparticles were collected in a tube from the outlet. The flow rate ratio was equal for all experiments. Three types of microchannels implemented to produce nanoparticles, included simple, active, and passive microchannels. A simple microchannel had a straight channel for fabricating nanoparticles. Active microchannel was used with high-frequency ultrasound to increase mixing efficiency in the channel. This microchannel was immersed in a water container equipped with two ultrasound wave transducers (1.7 MHz, model ANN-2517GRL, Annon Piezo Technology Co. Ltd., China). Passive microchannel used a wire coil to increase turbulence and thereby enhance mixing.

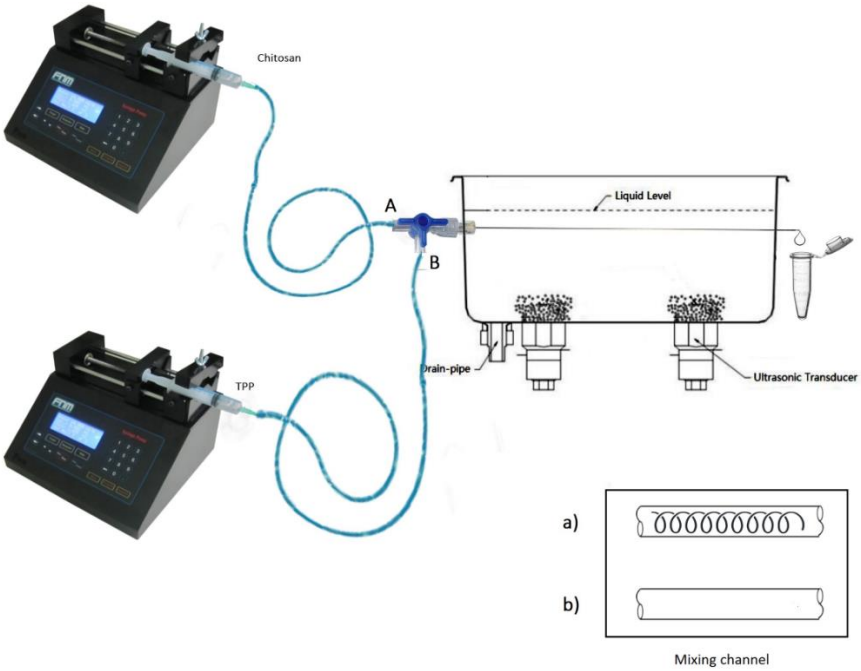

Fig. 1. A schematic view from experimental setup; (a) passive microchannel and (b) active or simple microchannel.

The nanoparticle size, PDI, and their zeta potential were measured using a zetasizer (Zetasizer, Nano-ZS Malvern Instrument Ltd., Worcestershire, UK). Nanoparticles were assessed using the red laser at a wavelength of 632.8 nm. All dynamic light scattering (DLS) measurements were carried out at 25 °C. Morphological structures of CS/TPP nanoparticles and the number of nanoparticles were obtained by scanning electron microscopy (SEM; Hitachi SU-70 Pleasanton, CA).

Besides microfluidic systems, a batch system was used to investigate the kinetics of reaction without the effect of mixing. This system provides sufficient mixing, which means the nucleation and growth rate kinetics are no longer dependent on the flow rate. CS and TPP solutions were prepared in different concentrations. TPP solution was added to stirring CS solution dropwise, and the viscosity of the sample was measured at different times. In addition, SEM pictures were used to measure the kinetic constants for the nucleation rate and the growth rate in the microchannel. The size and number of nanoparticles were measured at various times and various concentrations to achieve the nucleation rate and growth rate.

Analytical methods

In order to identify the effect of parameters and microchannels on the synthesis of nanoparticles and optimize them, the design of the experiment was applied. The D-optimal design was chosen instead of standard classical designs to minimize the number of required experiments. In view of scientific literature about producing CS nanoparticles, it can be seen that pH, CS concentration, CS/TPP mass ratio, and molecular properties of CS influence the size of nanoparticles. In microfluidic systems, the total flow rate and the type of microchannel are effective in mixing performance. So, in this work, the effect of four factors was investigated on the size and polydispersity of nanoparticles. CS concentration, CS/TPP mass ratio, and total flow rate were regarded as numerical factors and the type of microchannel was considered as a categorical factor. Table 1 illustrates the ranges and levels of studied process variables.

In the synthesis of CS/TPP nanoparticles in literature, the mass ratio of CS:TPP varies between 1:1 to 1:5. The mass ratio in this work was chosen by evaluating samples with different concentrations of CS and TPP. Samples were categorized by visual observation, including clear solution, opalescent suspension, and aggregates. A clear solution obtained in low concentrations, is an indication of very small particles which cannot be collected by centrifugation. Aggregate is refered to as the samples with large structures. While opalescent suspensions show the desired particles. In CS/TPP mass ratios higher than 3, clear solutions were observed in all samples. By examination of different CS concentrations, it was observed that at concentrations higher than 1 mg/mL, microstructures were detected at the output of simple microchannel (aggregate). Therefore, 1 mg/mL was considered as the maximum level of CS concentration to produce nanoparticles to avoid particle aggregation. The mass ratio was chosen between 1:1 to 1:3. The mathematical model is depicted by the following equation:

$$Y = \beta_0 + \sum_{i=1}^{k} \beta_i X_i + \sum_{i=1}^{k} \beta_{ii} X_i^2 + \sum_{j=1}^{k-1} \sum_{i=j-1}^{k} \beta_{ij} X_i X_j \qquad (1)$$

where, Y is the size or PDI of nanoparticles, β_0 is offset term, βi, βij, and βii are regression coefficients, and X_i and X_j are the uncoded independent variables. A credible procedure to analyze and determine the degree of certainty of experimental data is the analysis of variance (ANOVA) (29). The response variables (size and PDI) were fitted with the quadratic regression model to find a good relationship between the size and PDI and the other variables. The coefficients of determination and the analysis of variance were utilized to study the quality of the model.

Table 1. Experimental range and levels of the independent variables.

Variables	Symbols	Coded levels		
		-1	**1**	**1**
Chitosan concentration (mg/mL)	A	0.1	0.55	1
Total flow rate (mL/h)	B	4	12	20
Chitosan/tripolyphospate mass ratio	C	1	2	3
Type of microchannel	D	simple	active	passive

CFD simulation

Population balance method and reactive kinetics

Nanoparticles are formed by several processes, including nucleation and growth. Therefore, the population balance model was used to model the formation of nanoparticles (31). The general population balance method is written in term of particle disregarding aggregation and breakage terms is established as follows (32):

$$\frac{\partial n(L;\vec{x},t)}{\partial t}+\nabla.[\vec{v}_s n(L;\vec{x},t)]=-\frac{\partial}{\partial L}[G(L)n(L;\vec{x},t)] \quad (2)$$

where, n(L; $\vec{x}$, t) is the number density function, $\vec{v}_s$ is the particle velocity vector that is considered for all particles in this work, and G(L)n(L; $\vec{x}$, t) is the particle flux by the molecular growth rate. The nucleation rate is introduced through a boundary condition as follows:

$$n(L=0;\vec{x},t)G(L)=n_0 \quad (3)$$

where, n_0 is the nucleation rate.

In this work, the discrete method with 21 bins was preferred over the quadrature method of moments (QMOM) because the experimental size distribution was already known. The Sauter mean diameter was applied to calculate the particle diameter of nanoparticles, as follows:

$$d_{32}=\frac{\sum n_i d_i^3}{\sum n_i d_i^2} \quad (4)$$

The main problem with the modeling of CS nanoparticles was that there is no defined correlation between nucleation and growth rates. Figure 2 shows the progress of CS/TPP nanoparticles formation in the microchannels. Cross-link bonds occurred between amine groups in CS structure and phosphate groups in TPP and led to the formation of a nuclear and then nanoparticle.

Since ionotropic reaction leads to nanoparticle formation, the reactive kinetics plays a key role in numerical simulation. de Carvalho *et al*. (25) suggested a 1:3.3 stoichiometry at a molar ratio of TPP/CS_{mon} = 0.3. Then the nucleation reaction processes were simplified as:

$$3.3CS_{mon}+TPP\xrightarrow{k_n}nuclea \quad (5)$$

These two kinds of reactions were considered that follow certain classical kinetics. Therefore, the nucleation and growth rates can be introduced as follows:

$$n_0=k_n\,[CS_{mon}]^{3.3}[TPP] \quad (6)$$

$$n_0=k_n\,[CS_{mon}]^{3.3}[TPP] \quad (7)$$

$$G(L_i)=k_g\,[CS_{mon}]^{3.3}[TPP]\,[nuclea] \quad (8)$$

where, k_n and k_g are the nucleation and growth kinetic constants, respectively.

In addition, CS_{mon} and TPP are the concentrations of the monomer of CS and TPP molecules that freely dispersed in the liquid phase, and nuclea shows the concentration of solid molecule formed by equation (5). Both nucleation and growth rates were introduced to FLUENT using user-defined functions. In order to find the kinetic constants, various concentrations were evaluated in the constant molar ratio and the size and number of particles were measured.

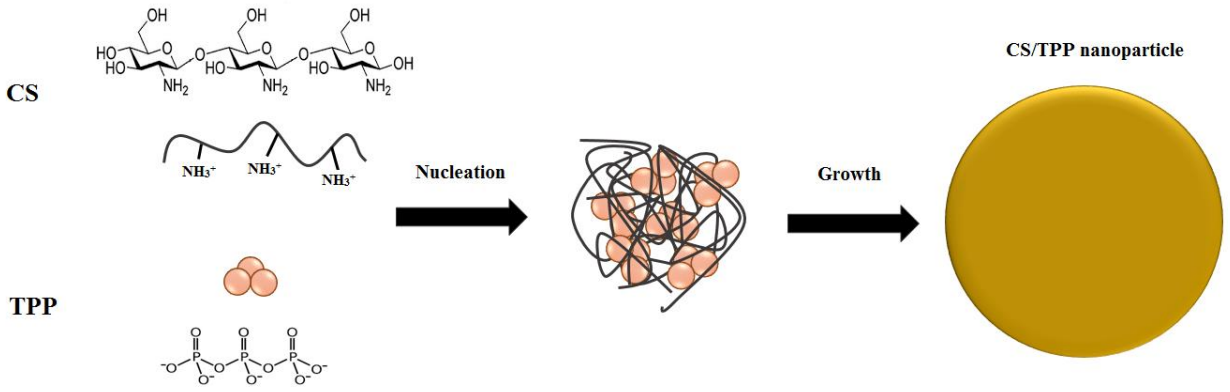

Fig. 2. The progress of CS/TPP nanoparticles formation in the microchannels. CS/TPP, Chitosan/tripolyphosphate.

CFD model

Three-dimensional geometries were created in a finite set of control volumes for all microchannels using GAMBIT software. Models consist of two cylinders with different sizes and lengths that are set to each other. For passive microchannel, wire coil was subtracted from the computational domain. As a routine method, in order to ensure the accuracy of the CFD simulations, a mesh independence study was performed. For this purpose, mixing quality at the outlet was considered in models in different numbers of control volumes. Mixing quality was defined based on uniformity of CS concentration in cross-section of mixing channel and calculated from the following expression:

$$\alpha = 1 - \sqrt{\frac{\sigma_M^2}{\sigma_{Max}^2}} \tag{9}$$

in which σ^2_{Max} is the maximum variance of the concentration and σ^2_M is determined as follows:

$$\sigma_M^2 = \frac{1}{n}\sum (C_{iN,Exp} - C_M)^2 \tag{10}$$

where, n and C_M are the numbers of cell points inside the cross-section of the microchannel and the perfect mixing concentration. Various meshes have been investigated with different mesh schemes and sizes. Finally, the computational domain was meshed using the tetrahedral scheme as the volumetric structure (because of the specific geometry of passive microchannel). Table 2 shows the pressure drops of different grid schemes with a flow rate of 4 mL/min in the passive microchannel. It can be seen that for finer mesh than 2.0×10^6 cells, grid size will have no significant effect on the calculation results. So, in order to consider the simulation cost, the tetrahedral scheme includes 2.0×10^6 cells were selected as the simulation structure.

Table 2. Different grid schemes and simulation

Number of meshes	Mixing quality	Error (%)
0.53×10^6	0.4326	
1.2×10^6	0.6343	31.79
1.7×10^6	0.7211	12.03
2.0×10^6	0.7806	7.62
2.3×10^6	0.797	2.1
2.7×10^6	0.8072	1.3

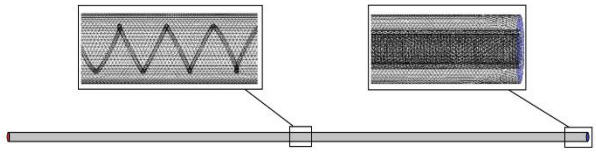

Fig. 3. Computational domain and cell structures of the passive microchannel.

Figure 3 reveals the computational volume domain and cell structures in the passive microchannel. Ansys 19 (Ansys Inc. USA) was applied to simulate nanoparticle formation in the microchannels. Two phases of flow (liquid-solid) were considered in the computational volume. The eulerian model was employed as a proper multiphase model in solving the PBM using the CFD Module. The liquid phase was considered as the primary phase, whereas nanoparticles were considered as the dispersed phase. The main equations of the Eulerian model for phase i is defined as:

Continuity equation:

$$\frac{\partial}{\partial t}(\alpha_i \rho_i) + \nabla.(\alpha_i \rho_i \vec{u}_l) = \sum_{p=1}^{2}(\dot{m}_{pi} - \dot{m}_{ip}) \tag{11}$$

Momentum equation:

$$\frac{\partial}{\partial t}(\alpha_i \rho_i \vec{u}_l) + \nabla.(\alpha_i \rho_i \vec{u}_l \vec{u}_l) = -\alpha_i \nabla P - \nabla.\bar{\tau}_i + \alpha_i \rho_i \vec{g} + \sum_{p=1}^{2}(\vec{R}_{pl} + \dot{m}_{pl}\vec{u}_{pl}) + (\vec{F}_i + \vec{F}_{lift,i} + \vec{F}_{vm,i}) \tag{12}$$

Energy equation:

$$\frac{\partial}{\partial t}(\rho E) + \nabla.(\vec{u}(\rho E + p)) = \nabla.(k_{eff}\nabla T - \sum_j h_j \vec{J}_j + (\overline{\overline{\tau_{eff}}}.\vec{u})) \tag{13}$$

where, $\vec{u}_l$ and $\dot{m}_{pi}$ are the velocity of phase i and mass transfer from the p[th] phase to i[th] phase, respectively. In addition, $\overline{\overline{\tau}}_i$, $\vec{F}_i$, $\vec{F}_{lift,i}$, $\vec{F}_{vm,i}$, and $\vec{R}_{pi}$ are the i[th] phase shear stress, external body force, lift force, virtual mass force, the interaction between phases, respectively. P represents the pressure and $\vec{u}_{pl}$ is the velocity between phases and may have two values:

$$\text{if } \vec{m}_{pi} > 0 \Rightarrow \vec{u}_{pl} = \vec{u}_p \tag{14}$$

$$\text{if } \vec{m}_{pi} > 0 \Rightarrow \vec{u}_{pl} = \vec{u}_p \tag{15}$$

k_{eff} is effective conductivity and its value is related to both phases. $\vec{J}_j$ is the diffusion flux of species. The physical properties of CS and TPP solutions were measured experimentally. Since diluted CS solutions were used in the

microchannels, the viscosity of solutions was modeled as a Newtonian fluid. Also, the diffusion coefficient was considered 10^{-9} for species. Velocity inlet and pressure outlet were considered for inlets and outlet, respectively. Other boundaries were adjusted on the wall condition. For active microchannel, piezoelectric transducers were placed at the bottom of the mixing channel and made movements in the vertical direction, so gravitational force was considered in this modeling. In order to simulate the vibration of the wall due to ultrasonic waves in the microchannel, the dynamic mesh was implemented. A user-defined function was joined to the main program and was used to define the vibration as wall displacements (12). The equation of movement was determined as follows:

$$y(x,t) = A(t)\cos(\frac{2\pi x}{\lambda}) \quad (16)$$

$$A(t) = A_0 \sin(\omega t) \quad (17)$$

where, A_0 = 1.35 × 10^{-9} m and ultrasound frequency is 1.7 KHz (33). In order to find a proper model, the Reynolds number was calculated for all conditions. It was found Reynolds number (Re) in all conditions is lower than 2500, so the laminar flow was dominated by the fluid flow. However, in the active microchannel, ultrasonic vibration increased turbulence in the neighborhood of the wall, therefore, the laminar model was considered to be unsuitable. Since a fully turbulent condition did not happen in the microchannel, RNG k-ε model was proper than other k-ε models (34), as follows:

$$\frac{\partial}{\partial t}(\rho k) + \frac{\partial}{\partial x_i}(\rho k u_i) = \frac{\partial}{\partial x_j}(\alpha_k \mu_{eff} \frac{\partial k}{\partial x_j}) + G_k + G_b - \rho\varepsilon - Y_M + S_k \quad (18)$$

$$\frac{\partial}{\partial t}(\rho \varepsilon) + \frac{\partial}{\partial x_i}(\rho \varepsilon u_i) = \frac{\partial}{\partial x_j}(\alpha_\varepsilon \mu_{eff} \frac{\partial \varepsilon}{\partial x_j}) + C_{1\varepsilon}\frac{\varepsilon}{k}(G_k + C_{3\varepsilon}G_b) - C_{2\varepsilon}\rho\frac{\varepsilon^2}{k} - R_\varepsilon + S_\varepsilon \quad (19)$$

G_k, G_b, and Y_M are the generations of turbulence kinetic energy due to the mean velocity gradients, the generation of turbulence kinetic energy due to buoyancy, and the contribution of the fluctuating dilatation in compressible turbulence to the overall dissipation rate, respectively. In addition, α_k and α_ε represent the inverse effective Prandtl numbers for k and ε, respectively.

Microchannel models assume an unsteady state, incompressible flow, governed by continuity, Navier-Stockes, and mass transfer by convection-diffusion. The convergence criteria were selected to be 10^{-6} and 10^{-8} for all predicted variables and chemical components, respectively. In the solution controls, the SIMPLE pressure-velocity coupling algorithm, the standard pressure, and the second-order upwind discretization scheme was set for momentum and mass transfer.

RESULTS

Twenty-eight experiments were done to get the experimental values of size and PDI. A second-order polynomial equation was implemented using the D-optimal method to verify the factor interactions and optimize the parameters. The summary of ANOVA is presented in Table 3. The quadratic regression model was chosen to predict responses. The associated probability (*P*) values less than 0.05 imply model terms are significant. The values of regression coefficient R^2 and the adjusted coefficient (R^2adj.) for both responses were more than 0.995, indicating the good fitness and precision of the model. A, B, C, D, AB, AD, BC, BD, CD, A^2, and C^2 in size model, all terms in PDI model were significant. The models for both responses are expressed in terms of coded factors as follows:

$$\text{Size} = 375.42 + 116.54A - 23.81B - 2.01C + 51.60D[1] + 16.25D[2] + 10.56AB + 20.52AD[1] + 7.92AD[2] + 18.19BC + 2.23BD[1] + 4.20BD[2] + 2.97CD[1] + 7.35CD[2] - 45.24A^2 - 1.66C^2 \quad (20)$$

$$\text{PDI} = 0.39 + 0.099A - 7.713 \times 10^{-3}B + 0.011C + 0.089D[1] - 6.876 \times 10^{-3}D[2] - 0.013AC - 0.051A^2 + 4.976 \times 10^{-3}B^2 - 0.011C^2 \quad (21)$$

The size of polymer nanoparticles is one of the most important determinants in the control of drug release and cellular uptake of nanoparticles (35).

Effect of parameters on nanoparticle size

The concentration of CS played the most important role in the size of nanoparticles. At C_{CS} = 1 mg/mL, the size of nanoparticles was higher compared to other concentrations. In addition, the total flow rate had a linear and inverse relationship with the size of particles. The size CS nanoparticles decreased by increasing total flow rate. The type of

microchannel is an effective parameter on the size. The effect of CS concentration is less in the passive microchannel, due to higher turbulence intensity in this microchannel.

CS/TPP mass ratio has a prominent effect on particle size but varies in different flow rates. At Q_T = 20 mL/h, the size increased with enhancing CS/TPP mass ratio. While, at Q_T = 4 mL/h, size and CS/TPP mass ratio had an inverse relationship. As TPP concentration increased in the process, the particle size declined due to enhanced cross-linking density between polymer and TPP. The effect of CS/TPP mass ratio on size altered by improving mixing performance due to the total flow rate. At Q_T = 20 mL/h, CS and TPP solutions were mixed very well and reduced the size of particles. However, in the low flow rate, mixing performance decreased due to the decrement of turbulence. In addition, with increasing CS/TPP mass ratio, the effect of the total flow rate reduced on particle size.

Effect of parameters on PDI

PDI is an important parameter to control drug release. As mentioned before, when diluting CS and TPP solutions were mixed, nanoparticles were formed spontaneously. So, the mixing performance can be dominated by nanoparticle size and PDI. CS concentration had a remarkable effect on PDI. Based on equation 21, the quadratic term of CS concentration was enhanced by increasing the CS concentration, so the effect of CS concentration decreased in higher concentrations. As mentioned before, at high CS concentration, the more chains were placed in a particle. In the other hand, the viscosity of CS solution increased and declined turbulence within the microchannel. According to equation 21, there is a nonlinear inverse relationship between total flow rate and particle PDI. However, the effect of flow rate on PDI was less than the other parameters. Results showed with increasing the values of CS/TPP mass ratio, PDI value increased first and then decreased. By evaluating the interaction between CS concentration and the CS/TPP mass ratio, it can be concluded that the high values of CS/TPP mass ratio increased the PDI. However, this factor decreased the effect of CS concentration on PDI at CS/TPP mass ratio = 3. In addition, by increasing CS concentrations, maximum PDI was achieved at lower CS/TPP mass ratios. It seems less TPP molecules in this mass ratio can provide more control on producing nanoparticles.

Table 3. ANOVA for response surface quadratic model.

Responses	Sources	Sum of squares	Mean of square	F Values	*P* > F	
Size	Model	389878.4	25991.89	34261.27	< 0.0001	significant
	A	251918.8	251918.8	332067.3	< 0.0001	
	B	10845.94	10845.94	14296.60	< 0.0001	
	C	34.74273	34.74273	45.79620	< 0.0001	
	D	63276.57	31638.28	41704.08	< 0.0001	
	AB	1204.338	1204.337	1587.500	< 0.0001	
	AD	5970.243	2985.121	3934.844	< 0.0001	
	BC	3130.284	3130.283	4126.190	< 0.0001	
	BD	403.7128	201.8564	266.0774	< 0.0001	
	CD	877.1136	438.5567	578.0846	< 0.0001	
	A^2	7158.448	7158.448	9435.925	< 0.0001	
	C^2	9.442614	9.442614	12.44680	0.0042	
	Residual	9.103652	0.758637			
	Lack of fit	5.708652	0.815521	1.201063	0.4348	not significant
Polydispersity index	Model	0.36600	0.040666	10244.96	< 0.0001	significant
	A	0.19141	0.191413	48221.65	< 0.0001	
	B	0.00106	0.001064	268.2145	< 0.0001	
	C	0.00194	0.001947	490.4961	< 0.0001	
	D	0.12117	0.060587	15263.35	< 0.0001	
	AC	0.00209	0.002090	526.7606	< 0.0001	
	A^2	0.00941	0.009415	2371.960	< 0.0001	
	B^2	0.00008	0.000087	22.14907	0.0002	
	C^2	0.00045	0.000459	115.7801	< 0.0001	
	Residual	0.00007	0.000003			
	Lack of fit	0.00005.	0.000004	1.729295	0.2838	not significant

A, Chitosan concentration (mg/mL); B, total flow rate (mL/h); C, chitosan/tripolyphospate mass ratio; D,

Table 4. Conditions and responses for three optimum points.

Microchannels	A	B	C	Size (nm)			Polydispersity index		
				Predicted value	Experimental value	Error (%)	Predictedvalue	Experimental value	Error (%)
Passive microchannel	0.10	19.99	1.00	126.0	124.3	-1.37	0.116	0.112	-3.377
Active microchnnel	0.10	20.00	1.00	166.7	160.9	-3.58	0.191	0.190	0.77
Simple microchannel	0.10	20.00	1.01	191.9	193.2	0.679	0.288	0.230	2.48

A, Chitosan concentration (mg/mL); B, total flow rate (mL/h); C, chitosan/tripolyphosphate mass ratio

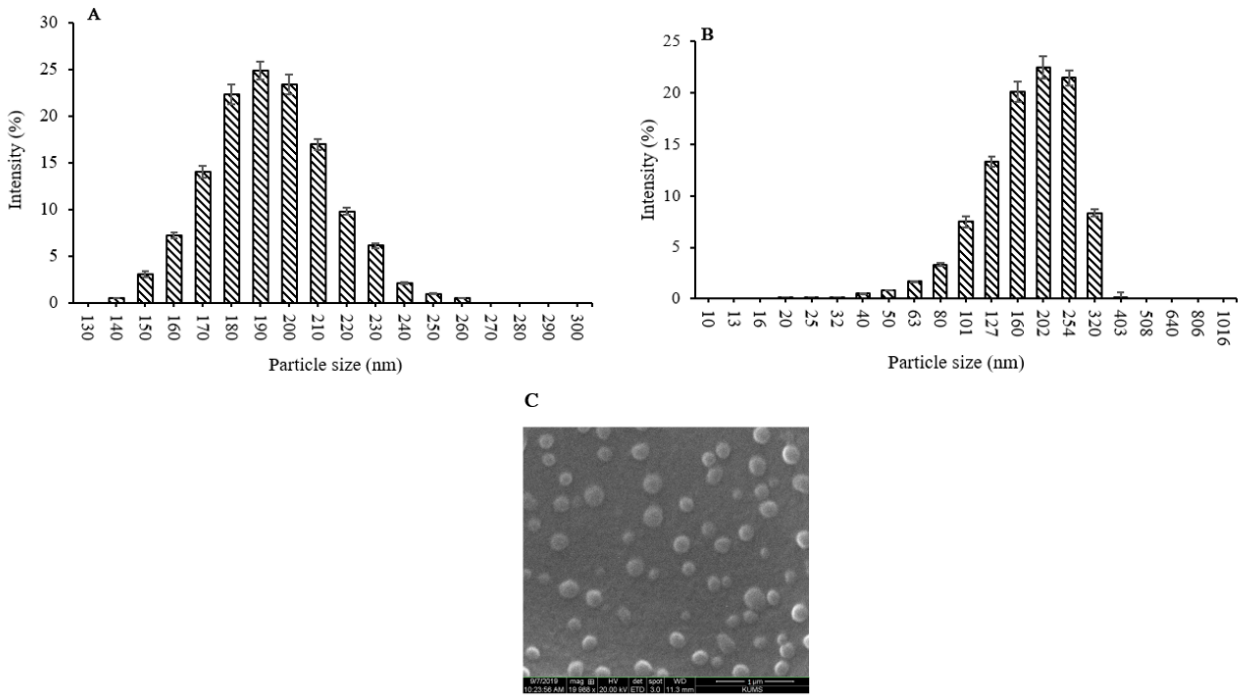

Fig. 4. A comparison between experimental and computational fluid dynamics results under the optimum condition for the simple microchannel. (A) Experimental particle size distribution, (B) simulated particle size distribution, and (C) scanning electron microscopy image of nanoparticles.

Process optimization

In this study, numerical optimization was applied based on equations 20 and 21 for each microchannel. The optimum conditions were calculated based on the minimum value of PDI and size. Table 4 presents conditions and responses for three optimum points. The table shows the minimum value for A and maximum values for B and C were used to find optimum points. Results showed the passive microchannel produced nanoparticles with proper size and PDI. According to the above results, the best-produced nanoparticles were formed by passive microchannel. At CS concentration of 0.1 mg/mL, the size of CS nanoparticles was 124 nm with PDI equal to 0.112, and +24.8 ± 4 mV zeta potential.

CFD results

CFD modeling was performed for the mixing pattern and fluid behavior analysis in all three microfluidic devices. In order to ensure validation of the model, the size and PDI of the nanoparticles in the microchannel were evaluated with the CFD model and experimental results for a simple microchannel. The maximum relative error between the CFD predicted and experimental measurement was considered 10%. Figure 4 depicts the nanoparticles produced by the optimum point of the simple microchannel. In this picture, CFD results and experimental results were compared. Nanoparticles SEM image was obtained, which is shown in Fig. 4C, indicating the nanoparticles had the average size of

193 nm and spherical shape. Size of nanoparticles achieved by CFD modeling is 227.3 (Error = 18%). In addition, experimental and numerical PDI were 0.23 and 0.31 (Error = 34%), respectively. Based on the results, modeling results were close to the experimental data, but not accurate enough. So, nucleation and growth rates needed some modification for achieving valid results.

In order to solve this problem, different concentrations of CS and TPP were tested to find the exact powers for equations 7 and 8. Results showed that the effect of TPP in growth rate is less than 1. Therefore, the power of TPP concentration decreased to 0.7.

In order to ensure modeling validity, the experimental and CFD results of nanoparticles produced by passive microchannel were compared under the optimum condition. Figure 5 illustrates the experimental and numerical results. Numerical results for size and PDI were 133.6 nm and 0.121, respectively. The difference between experimental and numerical results is less than 10%, so comparing results validates that CFD modeling can be implemented for the simulating process of producing nanoparticles. Coupling reactive kinetics and population balance method can help to study the effect of mixing into the microchannel.

Figure 6 shows the contours of CFD modeling in the simple microchannel. As shown in Fig. 6A, the ionic reaction happened where CS and TPP solutions mix. The reaction rate is fast, and the phase fraction of nanoparticles increased along the length of the microchannel, as shown in Fig. 6B. Nucleation and growth were happening along the microchannel and were increasing the phase fraction in the microchannel.

For each microchannel, velocity and concentration contours at a horizontal slice are illustrated in Fig. 7. A comparison between concentration contours shows CS solution is distributed over the entire width of the microchannel along the mixing channel. Besides, passive microchannel provided a good mixing performance due to interlacing streamlines and vortices. In addition, the flow path in this microchannel had a wave sinusoidal pattern due to the presence of the wire coil. As mentioned before, nanoparticles had a larger size and PDI in a lower flow rate. However, in a lower flow rate, the residence time increased which resulted in a better mixing. But in lower flow rate microchannel does not provide uniform concentration, good mixing, and leads to the formation of larger nanoparticles with higher polydispersity.

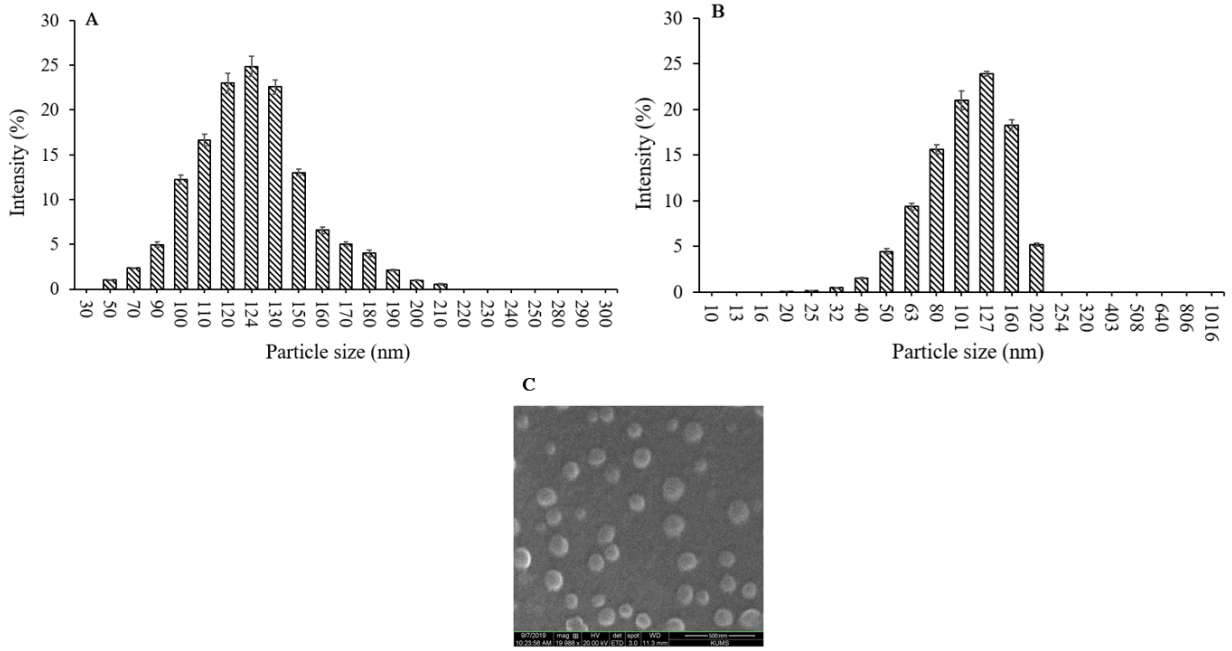

Fig. 5. A comparison between experimental and computational fluid dynamics results under the optimum condition for the passive microchannel. (A) Experimental particle size distribution, (B) simulated particle size distribution, and (C) scanning electron microscopy image of nanoparticles.

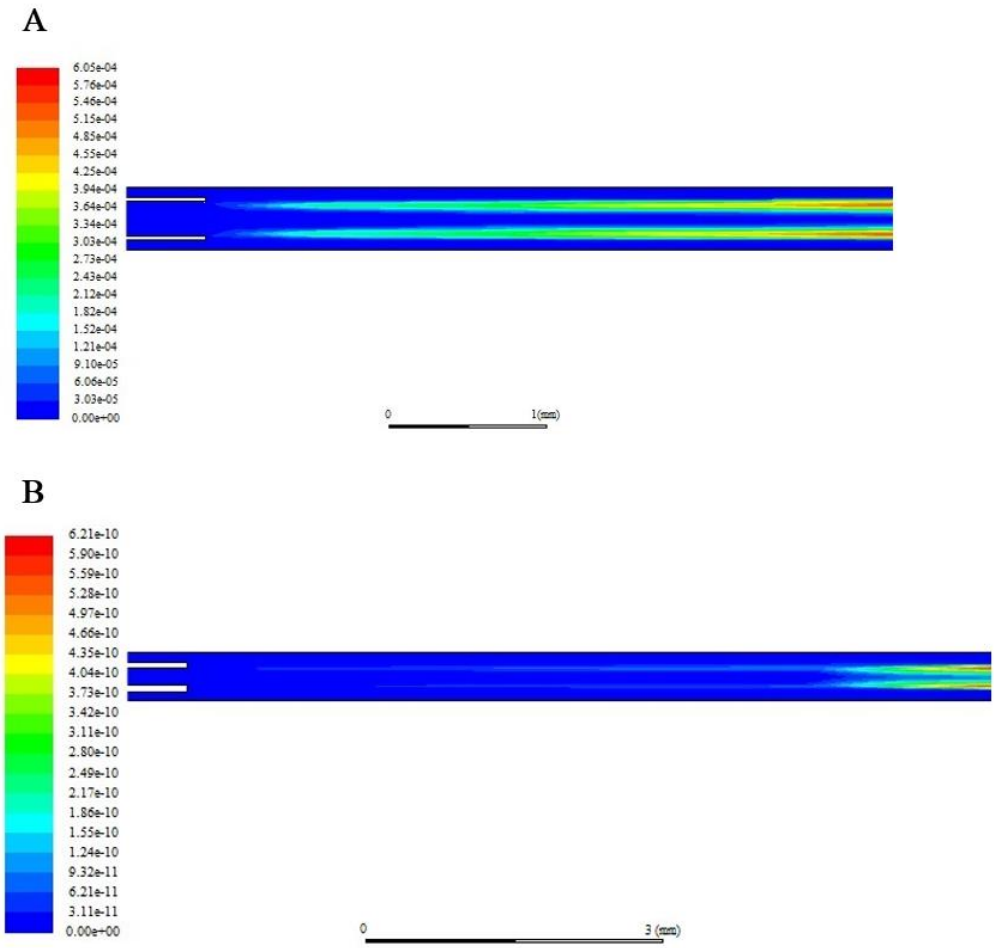

Fig. 6. Contours achieved by computational fluid dynamics modeling. (A) Contour of phase interaction and (B) contour of phase fraction of nanoparticles in simple channel.

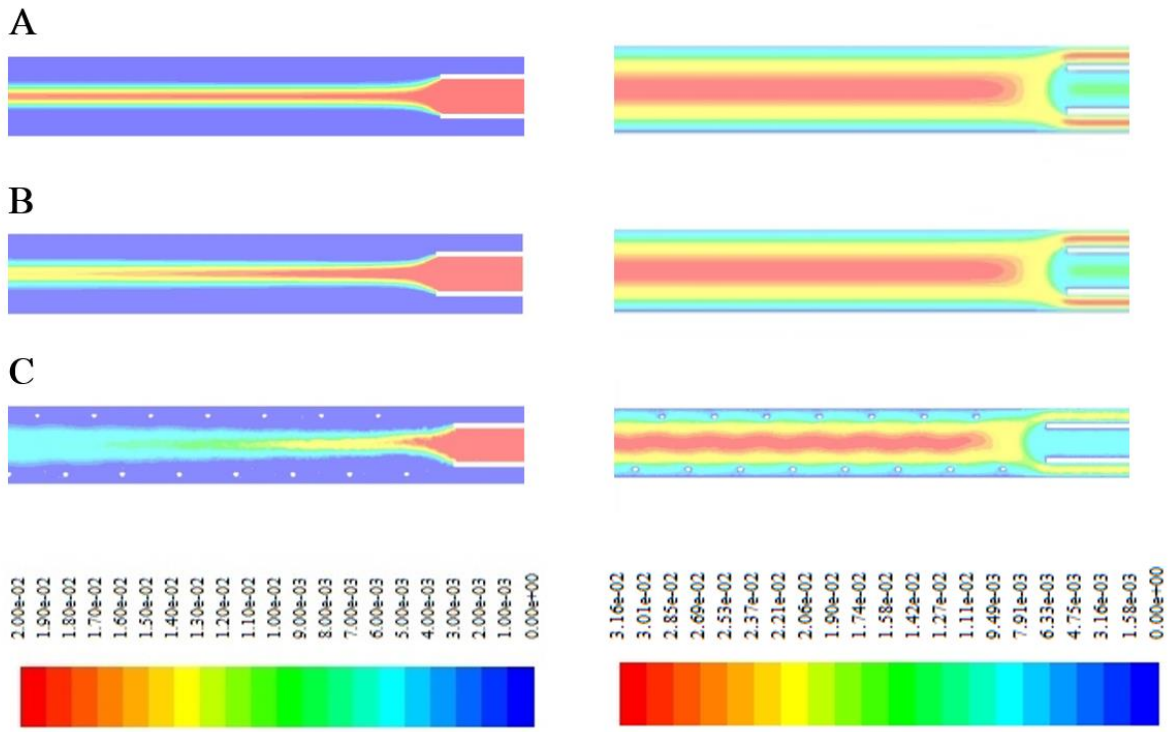

Fig. 7. Concentration and velocity contour in different microchannels (chitosan at 0.1 mg/mL, flow rate $_{(T)}$ = 4 mL/h). (A) Simple microchannel, (B) active microchannel, and (C) passive microchannel.

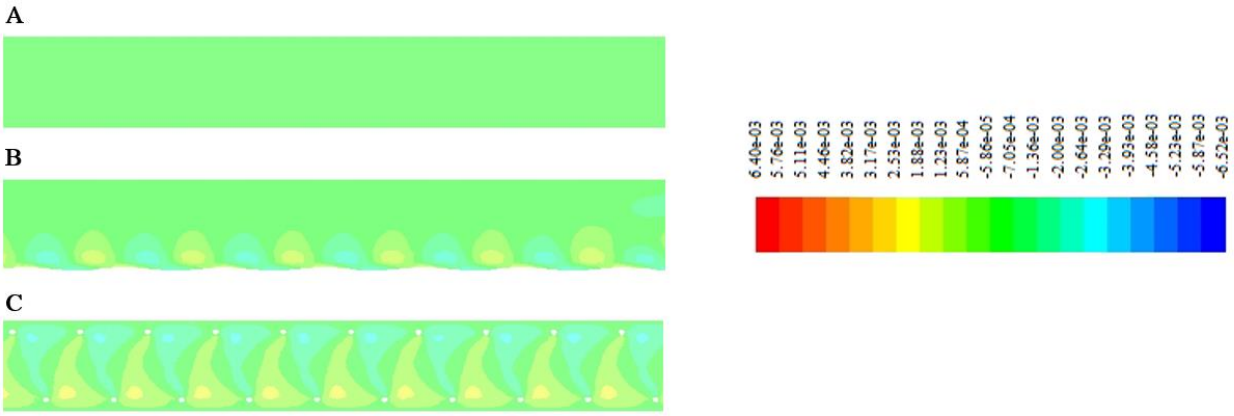

Fig. 8. The contour of movement velocity component (m/s) in different microchannels (chitosan at 0.1 mg/mL, flow rate $_{(T)}$ = 4 mL/h). (A) Simple microchannel, (B) active microchannel, and (C) passive microchannel.

Mixing performance increased in the active microchannel, but the effect of ultrasonic waves does not clear in this figure. Therefore, Y-direction velocity at a vertical slice that goes through the microchannel center line is presented in Fig. 8. As specified in this figure, ultrasonic waves influence y-velocity and make slight turbulence near the bottom of the microchannel. The ultrasound wave propagation makes a sinusoidal motion in the mixing channel. However, the effect of ultrasound propagation on mixing is quite obvious. In the passive microchannel, there are Y-direction velocity and Z-direction velocity in the whole of the microchannel. But, in the simple microchannel (Fig. 8A), the Y direction was almost zero. Figure 8 can explain the reason for better mixing in the passive microchannel. When flow hits the wire coil, it changes direction and creates vortices, although a simple microchannel has no significant movement in the Y and Z direction. The presence of vortices can decrease the diffusion path, enhance the contact surface between two fluids, and improve mixing in the channel.

DISCUSSION

CS/TPP nanoparticles are synthesized based on immediate linkages between phosphate and amino groups of CS. So, mixing plays an important role in the size and size distribution of CS/TPP nanoparticles by making homogeneity. While low ultrasonic irradiation could not decrease the size and PDI very effectively, high-frequency ultrasound is utilized to increase mass transfer and micromixing in the microchannel without effect on molecules integrity (11). Active and passive microchannels increase mixing intensity in a small volume and thereby provide more control.

The size of the particles heavily dependes on CS concentration. At higher CS concentration, more CS chains are next to each other and during the ionic gelation, more chains are placed in a particle. Similar variation was observed in whatever total flow rate. Turbulence intensity increased by enhancing the total flow rate, improved mixing in the channel, and produced smaller nanoparticles. CS concentration is more effective rather than the total flow rate. However, the effect of this parameter varies in different microchannels. The coil wire acts as an obstacle against the flow, enhances the turbulence, and declines the effect of viscosity and concentration of CS solution. Consequently, the effect of the total flow rate is more significant in passive microchannel compared to the other ones. The turbulence intensity respectively increased in simple, active, and passive microchannels. Therefore, the microchannel type influences the effect of CS/TPP mass ratio on particle size.

Simple and passive microchannels produced larger and smaller particles, respectively. Active microchannel provided better mixing compared to simple microchannel due to the presence of ultrasound. The range of high-frequency ultrasonic waves used in this work was able to increase micromixing and mass transfer due to making cavitation. Implosive

production and collapse of microbubbles created a variety of mechanical effects such as micro-streaming and micro-jet improve mass transfer in the microchannel. Simplicity in fabrication and low-pressure drop are the advantages of an active microchannel compared to the passive one (29). However, this microchannel cannot increase mixing as a passive one, nanoparticles produced with this microchannel can be regarded based on their applications. The fluid behavior of each method was evaluated using CFD modeling. CFD modeling showed flow behavior in three microchannels. In addition, CFD modeling can be used to find the size and PDI of nanoparticles in the microchannel. Nucleation and growth rates are predictable based on a reaction equation. CFD modeling of producing nanoparticles can be considered as a powerful tool for designing a process and evaluating it.

CONCLUSION

This work aimed to find a new method for modeling the process of producing polymeric nanoparticles and its application in predicting the size and PDI of nanoparticles for industrial purposes. Population balance method coupled with reactive kinetics was used to predict CS/TPP formation process. Microfluidic systems were selected as the continuous experimental systems. Different types of microchannels were used to investigate the formation of CS nanoparticles in the microchannel, including simple, active, and passive microchannels. CS/TPP reaction is considered a classic reaction and two equations were obtained for nucleation and growth rates. Experimental and numerical studies were combined to find the best approximation of size and PDI. The growth rate had a little change due to less TPP effect on the size of nanoparticles. Results were compared for all microchannels and showed that in microfluidic systems, mixing is an important parameter in nucleation and growth of nanoparticles. Active microchannel with increasing turbulence intensity and decreasing the diffusion path had the best performance compared to the other microchannels. The reactive kinetics was found very effective in the prediction of nanoparticle formation. By comparing the simulated results with the experimental results, the model was found to be in good agreement with the practice, leading to this method can be implemented to predict the size and PDI nanoparticles in different processes.

Acknowledgments

The authors gratefully acknowledge the Iran National Science Foundation (INSF; Grant No. 96016518) and Research Council of Kermanshah University of Medical Sciences (Grant No. 96508) for their financial supports.

Conflict of interest statement

All authors declared no conflict of interest in this study.

Authors' contribution

M. Akbari wrote the manuscript and carried out the experiments; Z. Rahimi wrote the manuscript and designed the experiments, and M. Rahimi performed CFD modeling.

REFERENCES

1. Bijari N, Ghobadi S, Derakhshandeh K. β-lactoglobulin-irinotecan inclusion complex as a new targeted nanocarrier for colorectal cancer cells. Res Pharm Sci. 2019;14(3):216-227. DOI: 10.4103/1735-5362.258488.
2. Mirzaei M. Effects of carbon nanotubes on properties of the fluorouracil anticancer drug: DFT studies of a CNT-fluorouracil compound. Int J Nano Dimens. 2013;3(3):175-179. DOI: 10.7508/IJND.2012.03.001.
3. Ahmadi F, Oveisi Z, Samani SM, Amoozgar Z. Chitosan based hydrogels: characteristics and pharmaceutical applications. Res Pharm Sci. 2015;10(1):1-16.
4. Mokhtari A, Harismah K, Mirzaei M. Covalent addition of chitosan to graphene sheets: density functional theory explorations of quadrupole coupling constants. Superlattices Microstruct. 2015;88:56-61. DOI: 10.1016/j.spmi.2015.08.031.
5. Amoozgar Z, Park J, Lin Q, Yeo Y. PH-responsive and macrophage evading low molecular weight chitosan coated nanoparticles for tumor-specific drug delivery. Res Pharm Sci. 2012;7(5):S991.
6. Anitha A, Sowmya S, Kumar PS, Deepthi S, Chennazhi K, Ehrlich H, *et al*. Chitin and chitosan in selected biomedical applications. Prog Polym Sci. 2014;39(9):1644-1667. DOI: 10.1016/j.progpolymsci.2014.02.008.

7. Bugnicourt L, Alcouffe P, Ladavière C. Elaboration of chitosan nanoparticles: favorable impact of a mild thermal treatment to obtain finely divided, spherical, and colloidally stable objects. Colloids Surf A Physicochem Eng Asp. 2014;457:476-486. DOI: 10.1016/j.colsurfa.2014.06.029.
8. Nasiri M, Azadi A, Hamidi M. Preparation of chitosan nanoparticles loaded by tramadol using ionic gelation method. Res Pharm Sci. 2012;7(5):S254.
9. Farokhzad OC, Langer R. Impact of nanotechnology on drug delivery. ACS Nano. 2009;3(1):16-20. DOI: 10.1021/nn900002m.
10. Patil A, Mishra V, Thakur S, Riyaz B, Kaur A, Khursheed R, *et al*. Nanotechnology derived nanotools in biomedical perspectives: an update. Curr Nanosci. 2019;15(2):137-146. DOI: 10.2174/1573413714666180426112851.
11. Faryadi M, Rahimi M, Akbari M. Process modeling and optimization of Rhodamine B dye ozonation in a novel microreactor equipped with high frequency ultrasound wave. Korean J Chem Eng. 2016;33(3):922-933. DOI: 10.1007/s11814-015-0188-6.
12. Rahimi M, Aghel B, Hatamifar B, Akbari M, Alsairafi A. CFD modeling of mixing intensification assisted with ultrasound wave in a T-type microreactor. Chem Eng Process. 2014;86:36-46. DOI: 10.1016/j.cep.2014.10.006.
13. Rahimi M, Akbari M, Parsamoghadam MA, Alsairafi AA. CFD study on effect of channel confluence angle on fluid flow pattern in asymmetrical shaped microchannels. Comput Chem Eng. 2015;73:172-182. DOI: 10.1016/j.compchemeng.2014.12.007.
14. Akbari M, Rahimi M, Fattahi A. Evaluation of microparticles formation by external gelationin a microfluidic system. Chem Eng Process. 2017;117:171-178. DOI: 10.1016/j.cep.2017.04.004.
15. Shokoohinia P, Hajialyani M, Sadrjavadi K, Akbari M, Rahimi M, Khaledian S, *et al*. Microfluidic-assisted preparation of PLGA nanoparticles for drug delivery purposes: experimental study and computational fluid dynamic simulation. Res Pharm Sci. 2019;14(5):459-470. DOI: 10.4103/1735-5362.268207.
16. Akbari M, Rahimi M, Faryadi M. Gas-liquid flow mass transfer in a T-shape microreactor stimulated with 1.7 MHz ultrasound waves. Chin J Chem Eng. 2017;25(9):1143-1152. DOI: 10.1016/j.cjche.2017.03.010.
17. Alvandimanesh A, Sadrjavadi K, Akbari M, Fattahi A. Optimization of de-esterified tragacanth microcapsules by computational fluid dynamic and the Taguchi design with purpose of the cell encapsulation. Int J Biol Macromol. 2017;105(Pt 1):17-26. DOI: 10.1016/j.ijbiomac.2017.06.059.
18. Jafarifar E, Hajialyani M, Akbari M, Rahimi M, Shokoohinia Y, Fattahi A. Preparation of a reproducible long-acting formulation of risperidone-loaded PLGA microspheres using microfluidic method. Pharm Dev Technol. 2017;22(6):836-843. DOI: 10.1080/10837450.2016.1221426.
19. Ansari M, Moradi S, Shahlaei M. A molecular dynamics simulation study on the mechanism of loading of gemcitabine and camptothecin in poly lactic-*co*-glycolic acid as a nano drug delivery system. J Mol Liq. 2018;269:110-118. DOI: 10.1016/j.molliq.2018.08.032.
20. Moradi S, Hosseini E, Abdoli M, Khani S, Shahlaei M. Comparative molecular dynamic simulation study on the use of chitosan for temperature stabilization of interferon αII. Carbohydr Polym. 2019;203:52-59. DOI: 10.1016/j.carbpol.2018.09.032.
21. Moradi S, Taran M, Mohajeri P, Sadrjavadi K, Sarrami F, Karton A, *et al*. Study of dual encapsulation possibility of hydrophobic and hydrophilic drugs into a nanocarrier based on bio-polymer coated graphene oxide using density functional theory, molecular dynamics simulation and experimental methods. J Mol Liq. 2018;262:204-217. DOI: 10.1016/j.molliq.2018.04.089.
22. Molaeian M, Davood A, Mirzaei M. Non-covalent interactions of *N*-(4-carboxyphenyl) phthalimide with CNTs. Adv J Chem B. 2020;2(1):39-45. DOI: 10.33945/SAMI/AJCB.2020.1.7
23. Wan B, Ring TA. Verification of SMOM and QMOM population balance modeling in CFD code using analytical solutions for batch particulate processes. China Particuology. 2006;4(5):243-249. DOI: 10.1016/S1672-2515(07)60268-1.
24. Jones A, Rigopoulos S, Zauner R. Crystallization and precipitation engineering. Comput Chem Eng. 2005;29(6):1159-1166. DOI: 10.1016/j.compchemeng.2005.02.022.
25. de Carvalho FG, Magalhães TC, Teixeira NM, Gondim BLC, Carlo HL, dos Santos RL, *et al*. Synthesis and characterization of TPP/chitosan nanoparticles: colloidal mechanism of reaction and antifungal effect on C. *albicans* biofilm formation. Mater Sci Eng C. 2019:109885,1-33. DOI: 10.1016/j.msec.2019.109885.
26. Pessoa AC, Sipoli CC, Lucimara G. Effects of diffusion and mixing pattern on microfluidic-assisted synthesis of chitosan/ATP nanoparticles. Lab Chip. 2017;17(13):2281-2293. DOI: 10.1039/C7LC00291B.
27. Majedi FS, Hasani-Sadrabadi MM, VanDersarl JJ, Mokarram N, Hojjati-Emami S, Dashtimoghadam E, *et al*. On-chip fabrication of paclitaxel-loaded chitosan nanoparticles for cancer therapeutics. Adv Mater Interfaces. 2014;24(4):432-441. DOI: 10.1002/adfm.201301628.
28. Dashtimoghadam E, Mirzadeh H, Taromi FA, Nyström B. Microfluidic self-assembly of polymeric nanoparticles with tunable compactness for controlled drug delivery. Polymer. 2013;54(18):4972-4979. DOI: 10.1016/j.polymer.2013.07.022.
29. Kamat V, Marathe I, Ghormade V, Bodas D, Paknikar K. Synthesis of monodisperse chitosan

nanoparticles and *in situ* drug loading using active microreactor. ACS Appl Mater Interfaces. 2015;7(41):22839-22847.
DOI: 10.1021/acsami.5b05100.

30. Calvo P, Remunan-Lopez C, Vila-Jato JL, Alonso MJ. Chitosan and chitosan ethylene oxide propylene oxide block copolymer nanoparticles as novel carriers for proteins and vaccines. Pharm Res. 1997;14(10):1431-1436.
DOI: 10.1023/a:1012128907225.
31. Bagheri H, Hashemipour H, Ghader S. Population balance modeling: application in nanoparticle formation through rapid expansion of supercritical solution. Comput Part Mech. 2019;6(4):721-737.
DOI: 10.1007/s40571-019-00257-w.
32. Shang X, Wan MP, Ng BF, Ding S. A CFD-sectional algorithm for population balance equation coupled with multi-dimensional flow dynamics. Powder Technol. 2020;362:111-125.
DOI: 10.1016/j.powtec.2019.11.084.
33. Hyun S, Lee DR, Loh BG. Investigation of convective heat transfer augmentation using acoustic streaming generated by ultrasonic vibrations. Int J Heat Mass Transf. 2005;48(3-4):703-718.
DOI: 10.1016/j.ijheatmasstransfer.2004.07.048.
34. Zhang J, Wang K, Lu Y, Luo G. Characterization and modeling of micromixing performance in micropore dispersion reactors. Chem Eng Process. 2010;49(7):740-747.
DOI: 10.1016/j.cep.2009.10.009.
35. Gan Q, Wang T, Cochrane C, McCarron P. Modulation of surface charge, particle size and morphological properties of chitosan-TPP nanoparticles intended for gene delivery. Colloids Surf B Biointerfaces. 2005;44(2-3):65-73.
DOI: 10.1016/j.colsurfb.2005.06.001.